Multi-decadal dynamics of the Saloum River delta mouth in climate change context

M. Sadio, I Sakho, M. Samou Seujip, A. Gueye, M. B. Diouf, Julien Deloffre

Version of Record: https://www.sciencedirect.com/science/article/pii/S1464343X22000036
Manuscript_63cde22aa7defb3437d88b2433b6e7b2

Multi-decadal dynamics of the Saloum River delta mouth in climate change context

SADIO, M. [1,2] ; SAKHO, I. [3,4] ; SAMOU SEUJIP, M.[3,5] ; GUEYE, A.[3] ; DIOUF, M.B. [5] ; DELOFFRE, J.[4]

[1]Laboratoire d'Enseignement et de Recherche en Géomatique (LERG), Ecole Supérieure Polytechnique, Université Cheikh Anta DIOP de Dakar, BP : 5085 Dakar - Fann, Sénégal :

[2]Laboratoire de Physique de l'Atmosphère et de l'Océan-Siméon FONGANG (LPAO-SF), Ecole Supérieure Polytechnique, Université Cheikh Anta DIOP de Dakar, BP : 5085 Dakar - Fann, Sénégal

[3]UMR Sciences, Technologies Avancées et Développement Durable, Université Amadou Mahtar MBOW de Dakar, 28, Lot Nord Liberté 6 VDN, BP 45927. Dakar – Senegal:

[4]UMR-CNRS 6143 M2C, Université de Rouen Normandie, Mont-Saint-Aignan, France:

[5] Laboratoire de Sédimentologie et de Biostratigraphie, Université Cheikh Anta DIOP de Dakar, BP : 5085 Dakar - Fann, Sénégal :

Multi-decadal dynamics of the Saloum River delta shoreline in a context of climate change

Abstract

The coast of Senegal is subject to climate variability that affects coastal dynamics. The Sangomar spit bounding the Saloum River delta provides a striking example. The spit dynamics has been characterized by complex changes involving both erosion and accumulation. Using a methodological approach combining remote sensing and data analysis in a Geographic Information System (GIS) we calculated a mean annual erosion rate of -3.55m of the spit shoreline from 1954 to 1987. In 1987 the spit was breached by storm in its most eroded sector (- 4.59m/year). This breach widened significantly to attain 5.25 km in 2018 and has now become the Saloum River mouth. The breach has resulted in exacerbated erosion of adjacent shorelines, especially at the down-drift coast, where the retreat attains a peak of -20.16m/year, the average erosion rate remaining at -3.56m/year for the entire coast. Extension of the spit tip has favoured progradation of the Sangomar Pointe which has lengthened by 5.74km between 1954 and 2018, diverting gradually the Saloum River former mouth towards the South, and corresponding to a 5,185,009m^3 sedimentation. Extrapolation of shoreline mobility reveals high erosion rates due to sea-level rise by 2050 and 2100.

Keywords: Coastal erosion, sandy spit, tidal inlet, climate change, Saloum River delta, Senegal

Introduction

Climate change and its consequences has become an active area of research for scientists (DENG et al., 2014). One of the consequences of climate change is global warming causing melting glaciers, rising sea levels and shoreline regression (KONKO et al., 2018). Shoreline retreat leads to coastal erosion with significant damage on socio-economic infrastructure and natural ecosystem (YANG et al., 2012; BAYRAM et al., 2013).

Previous studies indicate that many coastal African countries are highly vulnerable to climate change and sea-level rise, leading to increased rates of coastal erosion and flooding of low-lying coasts (IBE and AWOSIKA, 1991; DE LA VEGA-LEINERT et al., 2000).

Sea Level Rise (SLR) represents a threat for West Africa coastal communities and induce various coastal hazards such as storm surges, inundation of low-lying areas, beach erosion, and damage to coastal

infrastructure and ecosystems (NICHOLLS et al. 2007). The West African coastline is increasingly devastated by erosion and flood, causing loss of livelihood and environmental problems (NICHOLLS et al. 2008).

Several studies (UEMOA, 2010; IPCC, 2014; WACA, 2020) estimated that this coast will experience rates of sea-level rise considerably above the global average. This change, along with increased frequency of extreme weather events, will likely accelerate coastal erosion (SCHMIDT and MUGGAH, 2021).

In West Africa, the coastal zone focuses about 31% of the population and the main infrastructures (WACA, 2016). This area is exposed to several natural events that increase vulnerability and risk levels that have been recently highlighted by N'DOUR et al. (2017), ANTHONY et al. (2019), ALVES et al. (2020) and DADA et al. (2021), especially when the coastal sediment budget is impacted by anthropogenic activities such as coastal engineering and river dams. This coast is already facing storm surges, with intense winds and intense waves leading to coastal erosion (NIANG, 2012; ADDO, 2013). N'DOUR et al., (2018) analyzed the vicissitudes of the coast of Senegal regarding erosion. A particular point of vulnerability of this coast concerns the abundant spit systems that have formed at the mouths of both small rivers and the large Senegal River delta, reflecting the importance of waves and longshore transport in the dynamics of this coast (SADIO, 2017). Understanding how these spit systems evolve in a context of climate change, increased storminess, and coastal population growth is important in terms of coastal morphodynamics. But such approaches are also necessary in order to anticipate changes and population exposure to hazards. These spits have a protective role towards coastal communities by acting as barriers against waves and storms. They also participate in regulating estuarine dynamics through changes in inlet location and breaching, as shown by the example of the man-made breach across the Langue de Barbarie bounding the Senegal River delta, and the effects of which have been far-reaching in terms of coastal erosion (SADIO et al., 2017). These problems can be further compounded by sea-level rise, as anticipated over three decades ago by NIANG (1990). A fine present-day example is the Sangomar sandy spit in front of the Saloum River delta on the Petite-Côte of Senegal (fig. 1). This spit was breached on February 27, 1987, at Lagoba, in the course of strong northwest waves (DIAW et al., 1990; DIAW, 1997; THOMAS and DIAW, 1988). This breach gradually increased in size to become

one of the mouths of the Saloum River (THOMAS and DIAW, 2000), with morphodynamic implications on the adjacent shorelines (SADIO, 2017), and exposing the Saloum islands lying behind to the ocean storms, including erosion, overwash and flooding. Recent analysis of the Saloum River delta coast vulnerability to climate change reveals an increase of 3.2 mm/year in the sea level rise trend from 1993 to 2016, contributing thus to coastal vulnerability. It also states that exposure would increase in the future, in accordance with sea level rise and wave scenarios; which would further exacerbate coastal vulnerability, with potential bio-ecological and socio-economic impacts (SADIO et al., 2019).

The objective of this study is to analyze the multi-decadal dynamics of the Saloum River delta shoreline based on a remote sensing and Geographic Information Systems (GIS) approach. The shoreline mobility patterns are then extrapolated by 2050 and 2100 in order to gauge the longer-term risk associated with sea-level rise.

I. Study site

The Saloum River mouth has formed an embayed delta in the lee of a wave-controlled spit system between Diakhanor in the updrift end, and the Pointe de Sangomar in the downdrift sector (fig. 1) Geologically, the Saloum river catchment is part of the Senegal-Mauritanian basin, and is the net result of a climatic evolution characterized by five successive Late Quaternary geomorphological and sedimentological phases: submerged post-glacial ria, funnel-shaped estuary, barred estuary, cusped delta and finally “inverse” estuary (AUSSEIL-BADIE et al., 1991; BARUSSEAU, 1991; BARUSSEAU et al., 1993). Eustatic fluctuations and climatic oscillations have generated deposition phases including the construction of sandy beach ridges of which the Sangomar spit is an example (BOUCHET, 1998). The latest inverse estuary phase corresponds to a situation where freshwater inputs by the Saloum are less than the losses due to evaporation, a condition that generates hyperhaline water (PATUREJ, 2008). In some estuaries with very low fresh water inputs and particularly high evaporation rates, the increase in water density leads to a hypersaline density downwelling, resulting in a surficial water flow upwards, and a compensatory flow downwards near the bottom downwards (ALVERA-AZCARATE, 2011). In the case of the Saloum River, the increase is observed to be a roughly linear function of distance to the

90 sea (PAGES and CITEAU, 1989).

91

92 The Saloum mouth is mainly occupied by wetlands associated with a mosaic of islands and branching
93 channels called 'bolongs'. Three islands groups cover 80,000 hectares (BOUCHET, 1998). They are
94 separated by the three most important bolongs: the Saloum itself, the Diomboss and Bandiala. These
95 wetlands are essentially tidal. Mangroves (with few species) colonize mudflats and form continuous
96 belts around the islands (BOUCHET, 1998). Hypersaline areas devoid of mangroves, locally known as
97 ‘tannes’, extend from the back of these mudflats.

98

99 The tide is semi-diurnal along the entire coast of Senegal, and the range is microtidal (mean value of
100 1.70m, BOUCHET, 1998) in the Saloum. In Djiffère (fig. 1), the tide is flood-dominated and the annual
101 average amplitude is 0.627 m (high tide average is 1.2 m low tides average 0.570 m, with an amplitude
102 of 0.627 m). Tidal currents play a fundamental morphodynamic role by shaping the more or less
103 meandering bolongs and building sand bars generally located in front of the convex channel banks.
104 Tides also contribute to sedimentation at the mouth of the Saloum through the formation of an ebb delta
105 south of the Sangomar tip (BOUCHET, 1998).

106

107 The wave regime on the Senegalese coast is characterized by three main directions : waves from north-
108 northwest, waves from south-southwest and waves from west (fig 2).
109 The highest waves are from north-northwest, generated by westerly storms in the high latitudes of the
110 North Atlantic (GUILCHER, 1954) and trade winds in the Northern Hemisphere. These waves are
111 present throughout the year, but predominate mainly from mid-October to mid-July. According to the
112 WAVEWATCH III data, the average of significant waves height (Hs) reaches 2.6m (~5% reach 1.5m,
113 ~10% reach 2m (15%-5%), ~5% reach 2.5m (~20% -15%), 2% reach 3m (22%-20%), less than 1%
114 reach 4m (23% - 22%)). These waves generate a North-South longshore sediment transport on the coast
115 of Senegal that has been computed at 558 103 m3/year (SADIO et al., 2017) on the Langue de Barbarie
116 spit of the Senegal River delta.
117 Waves from south-southwest occur from July to October and are generated by the trade winds of the

118 southern hemisphere. Their average Hs amounts to 2.25m (~ 8% reach 1.5m, ~ 10% reach 2m (18% -
119 8%), ~ 1% reach 2.5m (19 % - 18%) and less than 1% reach 3 m (19.50% - 19%)). They shortly reverse
120 the direction of the longshore transport, with drift directed towards the north. Waves from a west window
121 may occur in October, November or December. These are relatively rare waves produced by storms and
122 hurricanes in the West Indies and the Caribbean Sea.
123
124 **II. Methodology**
125 The methodology is based on an approach involving remote sensing and Geographic Information
126 System (GIS) combined with statistical analysis using the Digital Shoreline Analysis System (DSAS,
127 THIELER et al., 2009) software application which runs on Esri's GIS:ESRI® ArcGIS 10.2 GIS. We
128 analyzed IGN vertical aerial photography, Corona satellite photography and Landsat satellite images,
129 from 1954 to 2018 (Table 1).
130
131 After the creation of composite bands, RGB (Red, Green, and Blue) composite raster drawing, pan-
132 sharpening (panchromatic image) and geometric verifications on Landsat satellite images, aerial
133 photography and satellite photography are georeferenced. The water line (swash line, run-up terminus)
134 was digitized. A statistical analysis of shoreline mobility was then performed using DSAS (version 4.3),
135 with choice of the Linear Regression Rate (LRR) which is the most robust method for measuring
136 historical trends in shoreline evolution (FENSTER et al., 1993).
137 Three potential error sources are taken into account in this analysis: the georeferencing error (RMS Root
138 Mean Square Error) named EG, the error resulting from the shoreline digitization, (EN) and that in
139 related to the tide oscillation (ED).
140
141 The EG error relating to georeferencing of IGN aerial photography and Corona satellite photography is
142 automatically calculated by the ArcGIS software which allowed this correction and is equal to 1 m.
143
144 In order to determine the EN margin of error resulting from digitization the first step is to choose a
145 shoreline for each spatial resolution. These chosen shorelines are then digitized (5 times each within a

few days), following the recommendations of COYNE et al. (1999) and FLETCHER et al. (2003). This repetition allowed the calculation of the average deviations in positioning of each shoreline, as well as the standard deviation of these deviations, as did FAYE (2010), FORD (2011; 2013) and SADIO (2017). The error arising from the digitization of each shoreline is obtained by adding the average of the deviations to 2 standard deviations of these deviations and to the pixel size (MOORE and GRIGGS, 2002):

EN = average + 2 standard deviations + pixel size. *Equation 1*

The ED error relating to the tide is determined using the ALLAN et al. (2003) formula, which geometrically calculates the D factor representing the shoreline position horizontal variability, and consecutive to a certain tidal height (M) on beach profile with a certain slope (tanβ), according to equation 2:

DHWL = M / tanβ. *Equation 2*

This formula, originally applied in the high water line (HWL) context was adapted by SADIO (2017) throughout Senegalese coast. Using this formula at instant shorelines (water line, swash line, runup terminus), DHWL becomes DWL; the ALLAN et al. (2003) formula becomes then DWL = M / tanβ (SADIO, 2017). For M, we choose the tidal range at the Dakar tide station (fig. 1), in absence of tide gauge data coinciding with the shooting dates. M is thus equal to 0.11 m. As for tanβ, it is to 6.39% according to field measurements.

The total shoreline position uncertainty (EP) is estimated according to COYNE et al. (1999) and FLETCHER et al. (2003) as the quadratic sum of each component (georeferencing, digitization and tidal oscillation), as shown in equation 3:

$$\boldsymbol{EP} = \sqrt{(\boldsymbol{E2_G} + \boldsymbol{E2_N} + \boldsymbol{E2_D})}. \qquad \textit{Equation 3}$$

Errors determined through Equation 3 correspond to a single image. When two shoreline positions extracted from two separate images (P1 and P2) are compared, the error becomes cumulative (ANDERS and BYRNES, 1991). Consequently, the total uncertainty for a given shoreline change rate estimated between two shoreline positions should be calculated taking into account both single errors and the time interval between the two photographs, so as to annualize the total error (FLETCHER et al., 2003, MORTON et al., 2004), using equation 4:

$$\boldsymbol{ERATE} = \sqrt{(\boldsymbol{E2} + \boldsymbol{E2})/\boldsymbol{T}} \quad \textit{Equation 4}$$

$$\boldsymbol{P1} \qquad \boldsymbol{P2}$$

where T is the time frame (in years) between the two photographs from which shorelines are extracted.

The total potential evolution rate error is thus achieved by solving equation 4 (Table 2).

In addition, volumetric analysis is carried out to complement the metric above. Based on the union of the 1954 and 2018 shorelines feature class polygons and the multiplication of the resulting area by the average topography from a 2018 Differential Global Positioning System (DGPS) survey, accretion becomes evident as one approaches the tip of the spit, as well as progradation of the Pointe de Sangomar. The potential error margin in the progradation volume is calculated by multiplying the error resulting from 1954 - 2018 shoreline mobility analysis (25.6 m) by 1 m, then by maximum error that can derived from the DGPS altitude (Z) which according to SUANEZ et al. (2008) is 1.28 cm. This calculation gives an error of 0.33 m^3.

To assess future shoreline evolution in response to climate change the historical trends were extrapolated as proposed by COOPER and PILKEY (2004). These authors suggest extrapolating the historically observed shoreline changes. Historical trends extrapolation assumes that future coastal evolution will be controlled by the same processes currently affecting the shoreline, namely the local influence of geology and geomorphology, waves, sea-level rise, sediment budgets and other important forcings. The other strength of this method is its applicability to a wide range of environments. THIELER et al (2001)

also argued that it is better to use historical observations and trends in beach evolution to predict the future. The two drawbacks of this method are: (1) the assumption that historical/current trends (e.g. sediment budgets, etc.) are representative of future trends, and (2) the need for long-term historical observations (spatial and temporal data) covering the study area which would not be skewed by natural or artificial short-term fluctuations (e.g. seasonal variability, building of coastal defense structures, etc.). Historical trends were computed from shoreline observations based on previous analysis, particularly that covering the period from 1987 to 2018, involving aerial photographs and satellite images. These historical trends were extrapolated by 2050 and 2100, using the following formula:

$$R_{futur} = R_{historical}, \quad \text{Equation 5}$$

with R refers to shoreline retreat.

The error margin included in these extrapolations has been estimated by extrapolating the one derived from the reference period. It would be 16 m for 2050 and 41 m for 2100.

III. Results and discussion

III.1. Multi-decadal evolution of the Saloum River Delta coast

The coast of the Saloum River delta experienced a major event in 1987, including the breaching of the Sangomar spit. The shoreline changes are analyze in two parts (i) before spit breaching (ii) after this event.

III.1.1. Multi- decadal shoreline evolution before the Sangomar spit breaching (from 1954 to January 1987)

The shoreline retreated from Ngalou Sessene to Niodior at a rate ranging from -4.59 to -0.65m/year (fig. 3). From -1.13m/year at Ngalou Sessene, the erosion became more significant towards the south, increasing to -1.47m/year at Palmarin, -2.13m/year at Diakhanor and -3.43m/year at Djffère. South of Niodior, there was gradual accretion that amounted to a maximum rate of 6.20 m/year. Shoreline retreat reached its maximum at Lagoba, with a rate of -4.59m/year. The spit segment related to this village, already highly weakened by erosion, was to become abruptly impacted and breached by an extreme

event, one month later, accentuating the shoreline retreat.

III.1.2. Multi-decadal shoreline evolution following the Sangomar spit breaching (from April 1987 to 2018)

During the period following spit breaching, notably from April 1987 to 2018, the shoreline underwent erosion from Ngalou Sessene to the outskirts of Niodior, from where accretion occured (fig. 4). Retreat increased overall from north to south, with -2.07m/year at Ngalou Sessene, -1.07m/year at Palmarin, -1.21m/year at Diakhanor and -2.37m/year at Djiffère. This retreat reached its highest rate at the beginning of the down-drift coast, south of the breach, with a maximum of -20.16m/year. Erosion then gradually decreased towards Niodior island, succeeded by accretion towards Pointe de Sangomar.

III.1.3. Evolution of the Lagoba breach, new mouth of the Saloum River

Following the breaching of the Sangomar spit, the breach gradually widened over several years, thus becoming new mouth of the Saloum River (fig. 5).

With a width of 277.81m just one month after the breaching, the breach constantly widened, at an average rate of 164m/year, reaching 5.25km in 2018. The widening of this breach also resulted in the opposite development of two other spits. Moreover, the spit the Sangomar spit tip gradually lengthened southward, thus diverting the former mouth of the Saloum River. From 1954 to 2018, the Pointe de Sangomar became elongated by 5.74 km (fig. 6).

This progradation of the spit tip occurred the addition of successive hooks (DIAW, 1998; THOMAS and DIAW, 2000; SADIO, 2017). It corresponds to a sand sedimentation of 5,185,009 m3. The widening of the breach exposed the villages on the mainland to the effects of waves and sea flooding.

III.1.4. Coastal erosion due to sea level rise (SLR) by 2050 and 2100

Historical trend extrapolation reveals similar trends to the current context, with erosion rates ranging

from -3.84 to -645.12m by 2050 and from -9.84 to -1653.12m by 2100, and accretion rates between 0.64 and 509.76m by 2050 and 1.64 and 1306.26m by 2100 (fig. 7). Thus, depending on the two target years considered, erosion would reach respectively -66.24 and -169.74m at Ngalou Sessene, -34.24 and -87.74m at Palmarin, -38.72 and -99.22m at Diakhanor, - 75.84 and -194.34m at Djiffère, -645.12 and -1653.12m south of the breach. As for accretion, it will progress increasingly from the section connected to Niodior towards Pointe de Sangomar. The average rate of change would be -32.72m for 2050 and -83.85 m for 2100.

The potential bio-ecological and socio-economic impacts of this shoreline retreat due to SLR would be:

- reworking of the spit and near- annihilation of its breakwater effect;
- disappearance of Djiffère village;
- large widening of the breach;
- direct exposure and erosion at Guimsam, Guissanor, Dionewar and Niodior islands;
- destruction of agriculture practiced in the islands due to massive tidal penetration;
- destruction of housing, tourist and hotel infrastructure established on the updrift coast (from Ngalou to Djiffère), especially Djiffère road.

III.2. Discussion

The shoreline evolution rates over the period preceding the breach (from 1954 to January 1987) are broadly similar to those obtained by SADIO (2017) over the same period. However, the average rate of change, -3.55 m/year, is higher than that of SADIO (2017) who obtained an annual average rate of -2.66 m. As for the period following the breach (from 1987 to 2018), the evolution rates are also generally similar to those measured by SADIO (2017) over a slightly shorter period, from 1987 to 2016.

The average rate of breach widening, 164 m/year, is lower than that of DIAW (1997) who measured 640m/year between 1987 and 1992, and THOMAS and DIAW (1997) who dertermined a rate of 470.85m/year from 1986 to 1993. This large difference could be justified by the time scales considered by DIAW (1997): 6 years and THOMAS and DIAW (1997): 7 years, which is shorter than the one used in the present study carried out at a multi-decadal scale (31 years), and especially by the fact that the breach widening rate was greater during the first years following the spit breaching.

However, the breach widening average rate remains higher than that of SADIO (2017): 124m/year from 1987 to 2016.

Compared to other coastal environments, shoreline erosion rates in the Saloum delta coast (over the period preceding the breach and for the period following the breach) are lower than those of the Nile delta coast, along which an erosion exceeding 50m/year has been computed (INMAN and JENKINS, 1984; FRIHY et al., 1991; NAFAA and FRIHY, 1991). They are also below the over 20 m/yr shoreline retreat recorded along the Danube delta coast (STANICA et al., 2011).

The retreat of the Saloum delta shoreline is as well less high than that of the Rhône delta coast (retreat of 15 m/yr measured by SABATIER and SUANEZ (2003) from 1895 to 2000) and the Pô delta coast (retreat of more than 10 m/yr monitored by the Council of Europe (2005) between 1954-1978), only over the period preceding the breach. However, for the period following the breach, the retreat of the Saloum delta shoreline is more significant than that of the coasts of the last two deltas mentioned.

Conclusion

Multi-decadal dynamics of the Saloum River mouth in climate change context is analyzed on the basis of remote sensing and Geographic Information Systems (GIS) approach and shoreline historical trends extrapolation. The results shows shoreline retreat between Ngalou Sessene and Niodior latitude, south of which gradual accretion occurs. Erosion reaches its highest rate at the spit segment named Lagoba village, where it breached in February 1987. Following this breaching shoreline dynamics displays erosion from Ngalou Sessene to Niodior outskirts, from where accretion proceeds. Likewise, the breach gradually widens over years, becoming thus the Saloum River new mouth, spit tip progradating gradually southward. Shoreline erosion due to sea level rise by 2050 and 2100 will increase, with potential socio-economic impacts; hence the need to think right now about the adaptation options to implement.

References

ADDO, K.A., 2013. Assessing the impact of sea-level rise on a vulnerable coastal community in Accra, Ghana. Journal of Disaster Risk studies, 5, 1.

ALLAN, J.C., KOMAR, P.D., and PRIEST, G.R., 2003. Shoreline variability on the high- energy Oregon coast and its usefulness in erosion-hazard assessments. Journal of Coastal Research, SI 38: 83-105.

ALVES, B., ANGNUURENG, D.B., MORAND, P., ALMAR, R., 2020. A review on coastal erosion and flooding risks and best management practices in West Africa: what has been done and should be done. J. Coastal Conservation, 24, 38,

ANDERS, F.J. and BYRNES, M.R., 1991. Accuracy of shoreline change rates as determined from map and aerial photographs. Shore and Beach, vol. 59, n°1, p. 17 - 26.

ANTHONY EJ, ALMAR R, BESSET M, REYNS J, LAÏBI R, RANASINGHE R, ABESSOLO ONDOA G, VACCHI M., 2019. Response of the bight of Benin (gulf of Guinea, West Africa) coastline to anthropogenic and natural forcing, part 2: sources and patterns of sediment supply, sediment cells, and recent shoreline change. Continental Shelf Research, 173, 93–103. https://doi.org/10.1016/j.csr.2018.12.006

AUSSEIL-BADIE, J., BARUSSEAU, J.-P., DESCHAMPS, C., DIOP, E.S., GIRESSE, P. and PADZUR, M., 1991. Holocene deltaic sequence in the Saloum estuary, Senegal. Quat. Research, Washington, vol. 36, pp. 178-194, 6 fig., 10 tabl.

BAYRAM, B., SEKER, D.Z., ACAR, U., YUKSEL, Y., GUNER, A.H.A. and CETIN, I., 2013. An Integrated Approach to Temporal Monitoring of the Shoreline and Basin of Terkos Lake. Journal of Coastal Research, 29, 1427-1435. https://doi.org/10.2112/JCOASTRES-D-12-00084.1

BOUCHET, L., 1998. L'évolution morphodynamique de la pointe de Sangomar (Sénégal) et ses conséquences sur le milieu. Mémoire de Maîtrise de Géographie. Université de Caen, 125 pages.

Conseil de l'Europe, 2005. Assemblée Parlementaire Documents de séance Session ordinaire. Protection des deltas européens. Volume 4, Documents 10534 à 10565, 261 p, ISSN 0252-0656.

COYNE, M.A., FLETCHER, C.H. and RICHMOND, B.M., 1999. Mapping coastal erosion hazard areas in Hawaii: Observations and errors. Journal of Coastal Research, Special Issue 28, p. 171 - 184.

DADA, O., ALMAR, R., MORAND, P., MENARD, F., 2021. Towards West African coastal social-

ecosystems sustainability: Intyerdisciplinary approaches. Ocean & Coastal Management, 211, 105746. https://doi.org/10.1016/j.ocecoaman.2021.105746

DE LA VEGA-LEINERT, AC., NICHOLLS, RJ., NASSER HASSAN, A., EL-RAEY, M., 2000. In: Proceedings of SURVAS expert workshop on: African vulnerability and adaptation to impacts of accelerated sea-level rise (ASLR). National Authority on Remote Sensing and Space Sciences (NARSS), Egypt, 104 pp. http://www.survas.mdx.ac.uk

DENG, H.J., CHEN, Y.N., SHI, X., LI, W.H., WANG, H.J., ZHANG, S.H. and FANG, G.H., 2014. Dynamics of Temperature and Precipitation Extremes and Their Spatial Variation in the Arid Region of Northwest China. Atmospheric Research, 138, 346-355. https://doi.org/10.1016/j.atmosres.2013.12.001

DIAW, A.T., 1997. Evolution des milieux littoraux du Sénégal. Géomorphologie et Télédétection. Thèse de Doctorat d'Etat ès Lettres, Université de Paris I / Panthéon - Sorbonne, Paris, 270 p.

DIAW, A.T., DIOP, N. and THOMAS, Y.F., 1990. Rupture of the spit of Sangomar. Estuary of the Saalum, Senegal. AIAA Series Progress, Washington, pp.

FAYE, I.B.N., 2010. Dynamique du trait de côte sur les littoraux sableux de la Mauritanie à la Guinée-Bissau (Afrique de l'Ouest) : Approches régionale et locale par photointerprétation, traitement d'images et analyse de cartes anciennes. Thèse de Doctorat de Géographie, Université de Bretagne Occidentale, Volume 1, 321 p.

FLETCHER, C.H., ROONEY, J.J., BARBEE, M., LIM, S.C. and RICHMOND, B., 2003.

Mapping shoreline change using digital orthophotogrammetry on Maui, Hawaii. Journal of Coastal Research, Special Issue n°38, p. 106 - 124.

FORD, M., 2013. Shoreline changes interpreted from multi-temporal aerial photographs and high resolution satellite images: Wotje Atoll, Marshall Islands. Remote Sensing of Environment, 135 130–140.

FORD, M., 2011. Shoreline changes on an urban atoll in the Central Pacific Ocean: Majuro Atoll, Marshall Islands. Journal of Coastal Research, 28, 11–22.

FRIHY, O.E., FANOS, M.A.; KHAFACY, A.A., and KOMAR, P.D., 1991. Nearshore sediment transport patterns along the Nile Delta, Egypt. Journal of Coastal Engineering, 15, 409-429.

INMAN, D.L., and JENKINS, S.A., 1984. The Nile littoral cell and man's impact on the coastal zone of the southeastern Mediterranean. Scripps Institution of Oceanography, Reference Series 84-31, University of California, La Jolla, 43p.

IPCC, 2014. “Synthesis Report Summary for Policymakers.”

KONKO, Y., BAGARAM, B., JULIEN, F., AKPAMOU, K.G. and KOKOU, K., 2018. Multitemporal Analysis of Coastal Erosion Based on Multisource Satellite Images in the South of the Mono Transboundary Biosphere Reserve in Togo (West Africa). Open Access Library Journal, 5, e4526. https://doi.org/10.4236/oalib.1104526

MORTON, R.A., MILLER, T.L. and MOORE L.J., 2004. National assessment of shoreline change: Part 1. Historical shoreline changes and associated land loss along the U.S. Gulf of Mexico. U.S. Geological Survey, Open-file report 2004-1043, 42 p.

NAFAA. M.G. and FRIHY, O.K. 1991. Beach and nearshore features along the dissipative coastline of the Nile River Delta, Egypt. Journal of Coastal Research, 9(2), 423-433. Fort Lauderdale (Florida), ISSN 0749-0208.

NDOUR, A., LAÏBI, R., SADIO, M., DEGBÉ, C.G.E., DIAW, A.T., OYÉDÉ, L.M., ANTHONY, E.J., DUSSOUILLEZ, P., SAMBOU, H., DIÈYE, E.H.B., 2018. Management strategies for coastal erosion problems in West Africa: Analysis, issues, and constraints drawn from examples from Senegal and Benin. Ocean & Coastal Management, 156, 92-106. https://doi: 10.1016/j.ocecoaman.2017.09.001.

NIANG, I. 2012. Coastal erosion and the adaptation to climate change in coastal West Africa. Adaptation and Mitigation Strategies, 249-250.

NIANG, I., 1990. Response to the impacts of green house induced sea level rise in Senegal. In TITUS, J.G. (Ed.), Changing Climate and the Coast, Volume 2, Washington D.C., National Academy of Press, 182 p.

.

NICHOLLS, R. J., S. HANSON, C. HERWEIJER, N. PATMORE, S. HALLEGATTE, J. CORFEE-MORLOT, J. CHÂTEAU, and R. MUIR-WOOD. 2008. Ranking port cities with high exposure

and vulnerability to climate extremes: Exposure estimates. OECD Environment Working Papers No. 1." doi: https://dx.doi.org/10.1787/011766488208.

NICHOLLS, R.J., P.P. WONG, V.R. BURKETT, J.O. CODIGNOTTO, J.E. HAY, R.F. MCLEAN, S. RAGOONADEN and C.D. WOODROFFE, 2007. Coastal systems and low-lying areas. Climate Change 2007: Impacts, Adaptation and Vulnerability. Contribution of Working Group II to the Fourth Assessment Report of the Intergovernmental Panel on Climate Change, M.L. Parry, O.F. Canziani, J.P. Palutikof, P.J. van der Linden and C.E. Hanson, Eds., Cambridge University Press, Cambridge, UK, 315-356.

PAGES, J. and CITEAU, J., 1989. Rainfall and salinity of a Sahelian estuary between 1927 and 1987, J. Hydrol, vol.113, pp.325-341.

PATUREJ, E., 2008. Estuaries – types, role and impact on human life, 37 p.

ROBINSON, E. et al. P.S. 2012. Shoreline changes and sea-level rise at Long Bay, Negril, western Jamaica. Caribbean Journal of Earth Science, Volume 43, 35-49. Available online: 2nd July 2012. Geological Society of Jamaica.

SABATIER, F. and SUANEZ, S., 2003. Evolution of the Rhône delta coast since the end of the 19th century/ Cinématique du littoral du delta du Rhône depuis la fin du XIXe siècle. In: Géomorphologie : relief, processus, environnement, Octobre-décembre, vol. 9, n°4. pp. 283-300; doi : https://doi.org/10.3406/morfo.2003.1191, https://www.persee.fr/doc/morfo_1266-5304_2003_num_9_4_1191

SADIO M., SECK A., NOBLET M., CAMARA I., 2019. Evaluation de la vulnérabilité du secteur de la zone côtière à la variabilité et aux changements climatiques dans la région de Fatick. Report produced under the project "Projet d'Appui Scientifique aux processus de Plans Nationaux d'Adaptation dans les pays francophones les moins avancés d'Afrique subsaharienne", Climate Analytics gGmbH, Berlin, 114 p.

SADIO, M., 2017. Morphodynamique et aménagement des flèches littorales de la côte du Sénégal. Thèse de Doctorat de Géographie Physique, Spécialité : Géomorphologie Littorale. Université Cheikh Anta Diop de Dakar et Aix - Marseille Université, 403 p.

SADIO, M., ANTHONY, E.J., DIAW, A.T., DUSSOUILLEZ, P. FLEURY, J.T., KANE, A., ALMAR, R., KESTENARE, E., 2017. Shoreline changes on the wave-influenced Senegal River delta, West Africa: The roles of natural processes and human interventions. Water, 9 (5), 357. doi:10.3390/w9050357

SCHMIDT, P. and MUGGAH, R., 2021. Assessing the relationships between climate change and security in west Africa. Igarapé Institute, 17 p.

STANICA, A., DAN, S., JIMENEZ, J.A. and UNGUREANU, G.V., 2011. Dealing with erosion along the Danube Delta coast. The CONSCIENCE experience towards a sustainable coastline management, Ocean & Coastal Management, Volume 54, Issue 12, Pages 898-906, ISSN 0964-5691, https://doi.org/10.1016/j.ocecoaman.2011.06.006.

SUANEZ, S., DEHOUCK, A. et STEPHAN, P., 2008. Incertitude de la mesure de terrain en géomorphologie littorale. Approche statistique et quantification des marges d'erreur. Société d'Écologie Humaine (SEH). Incertitude et environnement. La fin des certitudes scientifiques, ÉDISUD, pp. 127-139, Écologie Humaine. hal-00342887.

THIELER, E.R., HIMMELSTOSS, E.A., ZICHICHI, J.L., and ERGUL, A., 2009 Digital Shoreline Analysis System (DSAS) version 4.0 — An ArcGIS extension for calculating shoreline change: U.S. Geological Survey Open-File Report 2008-1278.

UEMOA (Union économique et monétaire d'Afrique de l'Ouest), 2010. Étude régionale de suivi du trait de côte et schéma direc¬teur du littoral de l'Afrique de l'Ouest. Diagnostic régional.

YANG, B., HWANG, C. and CORDELL, H.K., 2012. Use of LiDAR Shoreline Extraction for Analyzing Revetment Rock Beach Protection: A Case Study of Jekyll Island State Park, USA. Ocean & Coastal Management, 69, 1e15. https://doi.org/10.1016/j.ocecoaman.2012.06.007

West African Coastal Areas Management Program (WACA), 2020, "Rising Tide: Protecting Vulnerable Coastal Communities in West Africa | WACA." https://www.wacaprogram.org/article/rising-tide-protecting-vulnerable-coastal-communities-west-africa.

LIST OF FIGURE CAPTIONS

LISTE OF FIGURES


Ngalou Sam Sam
Ngalou Sessene
Nguedj
Palmarin
Diakhanor
Djifère
Dionouar
Niodior
Pointe Sangomar
Fatick
Foundiougne
Parc National du Delta du Saloum
Forêt Classée des Iles du Saloum
North Atlantic Ocean
Saint-Louis
Louga
Thies
Pikine
Dakar
Diourbel
Kaolack
Banjul
Sources : ESRI World Imagery, 2020

Figure 1

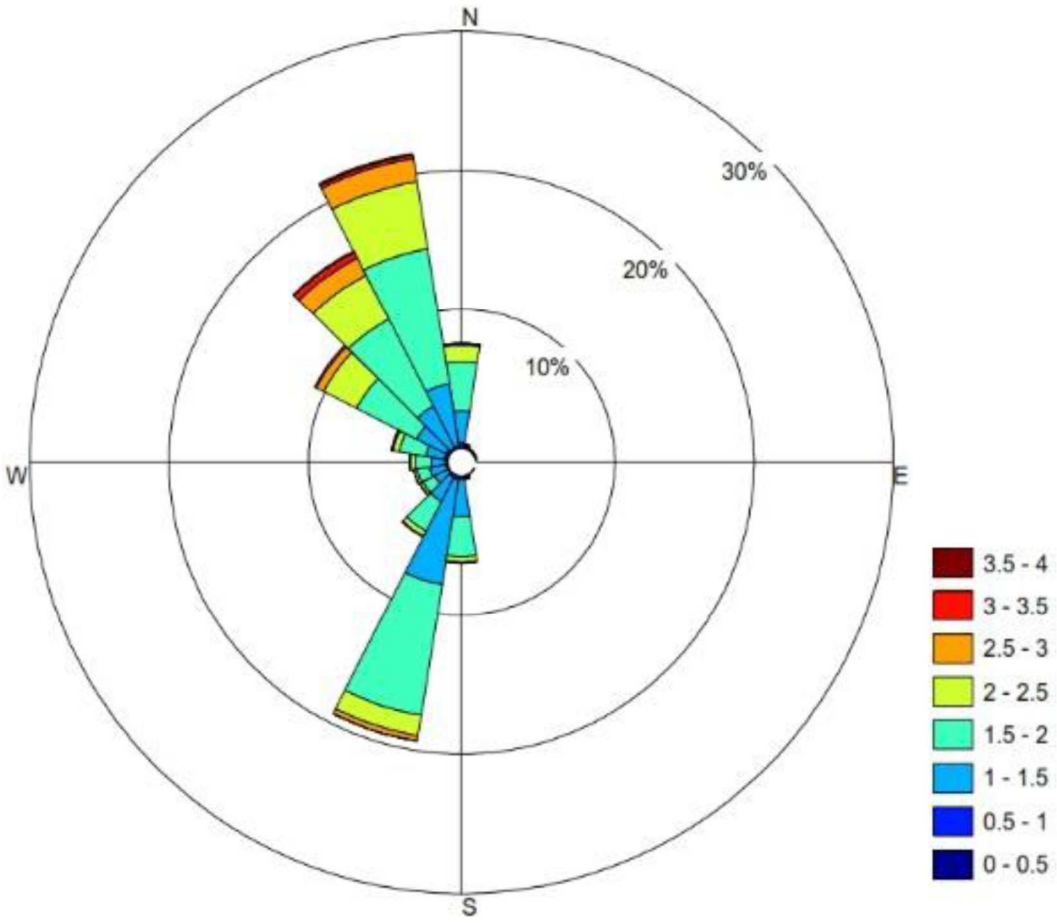

Figure 2

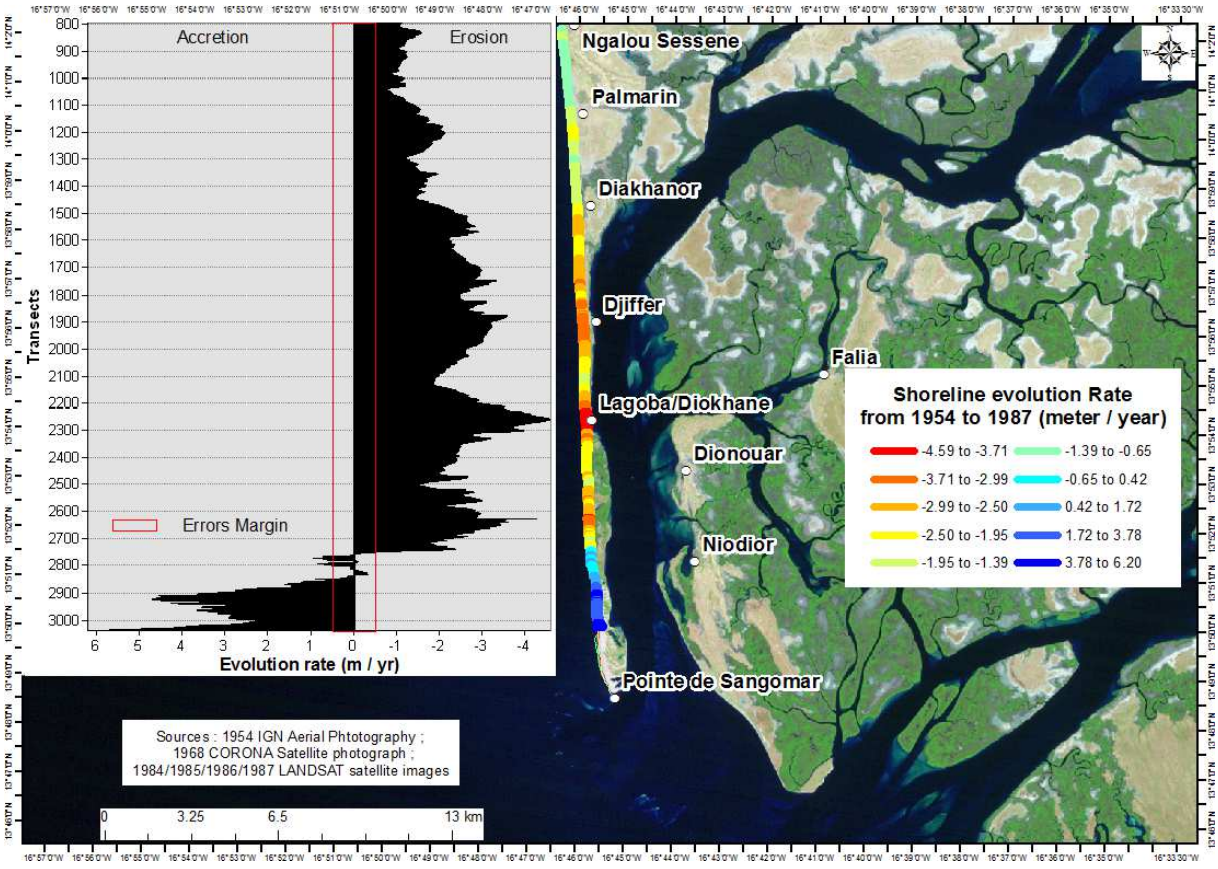
Accretion
Erosion
Transects
Errors Margin
Evolution rate (m / yr)
Ngalou Sessene
Palmarin
Diakhanor
Djiffer
Falia
Lagoba/Diokhane
Dionouar
Niodior
Pointe de Sangomar
Shoreline evolution Rate
from 1954 to 1987 (meter / year)
-4.59 to -3.71
-3.71 to -2.99
-2.99 to -2.50
-2.50 to -1.95
-1.95 to -1.39
-1.39 to -0.65
-0.65 to 0.42
0.42 to 1.72
1.72 to 3.78
3.78 to 6.20
Sources : 1954 IGN Aerial Phtotography ;
1968 CORONA Satellite photograph ;
1984/1985/1986/1987 LANDSAT satellite images
0
3.25
6.5
13 km

: *Figure 3*

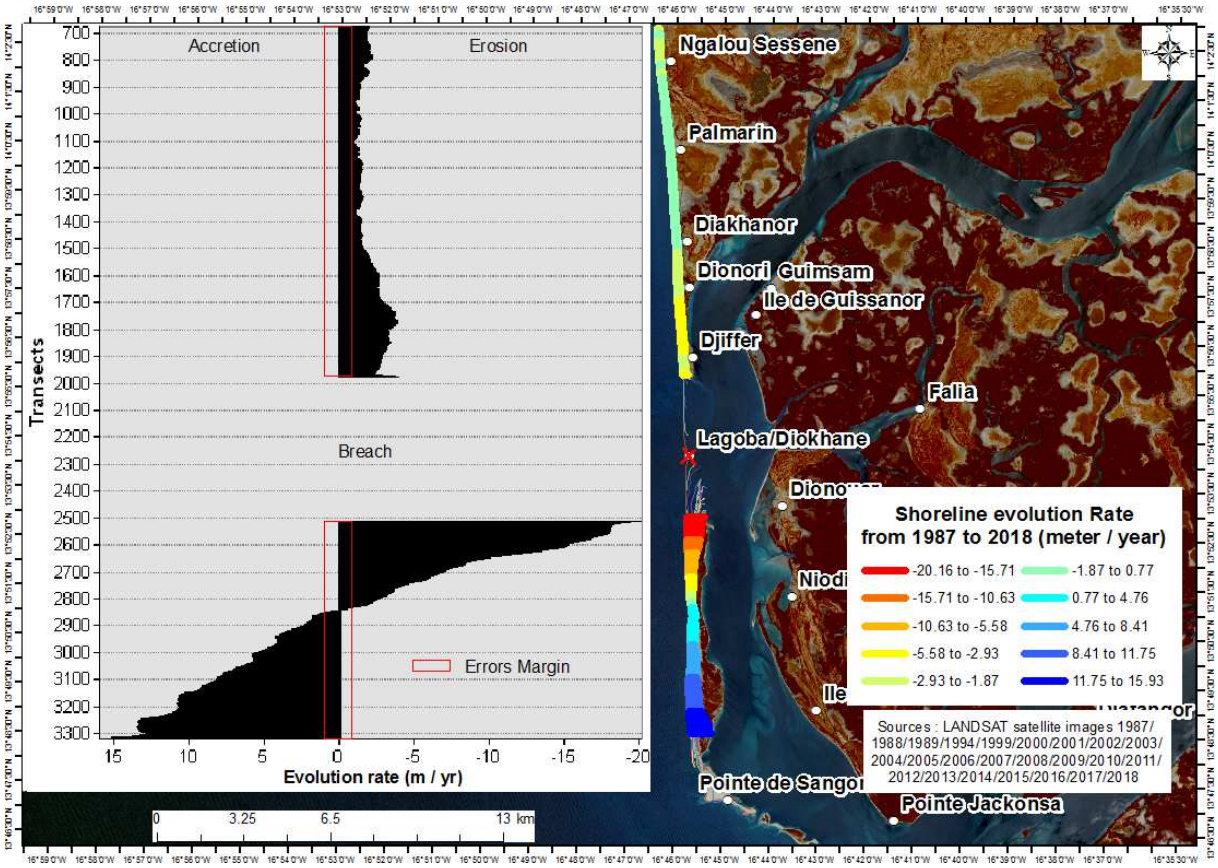
Accretion
Erosion
Breach
Errors Margin
Transects
Evolution rate (m / yr)
Ngalou Sessene
Palmarin
Diakhanor
Dionori Guimsam
Ile de Guissanor
Djiffer
Falia
Lagoba/Diokhane
Niodi
Pointe de Sangor
Pointe Jackonsa
Shoreline evolution Rate
from 1987 to 2018 (meter / year)
-20.16 to -15.71
-15.71 to -10.63
-10.63 to -5.58
-5.58 to -2.93
-2.93 to -1.87
-1.87 to 0.77
0.77 to 4.76
4.76 to 8.41
8.41 to 11.75
11.75 to 15.93
Sources : LANDSAT satellite images 1987/
1988/1989/1994/1999/2000/2001/2002/2003/
2004/2005/2006/2007/2008/2009/2010/2011/
2012/2013/2014/2015/2016/2017/2018
0
3.25
6.5
13 km

) Figure 4

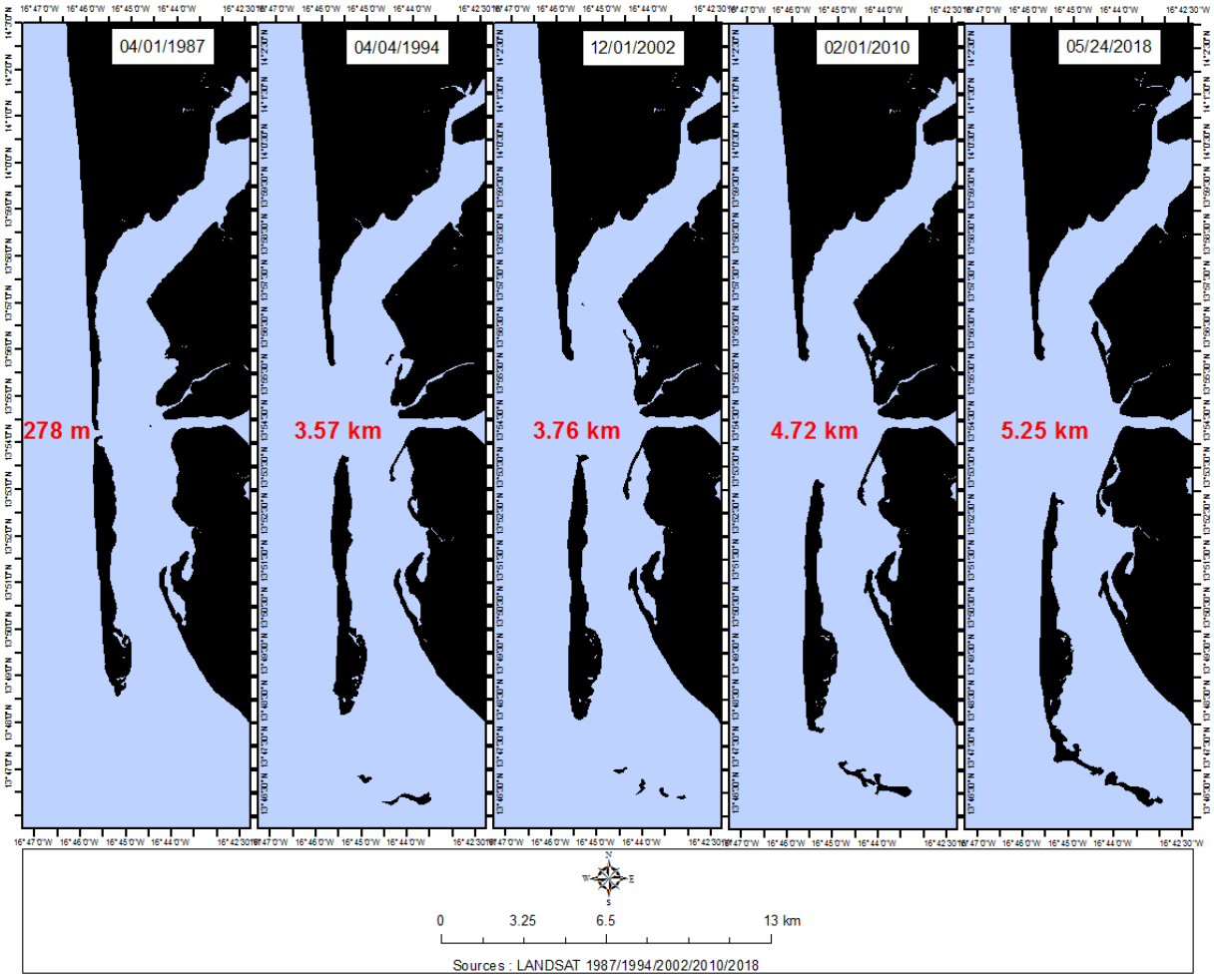
04/01/1987
04/04/1994
12/01/2002
02/01/2010
05/24/2018
278 m
3.57 km
3.76 km
4.72 km
5.25 km
0
3.25
6.5
13 km
Sources : LANDSAT 1987/1994/2002/2010/2018

Figure 5

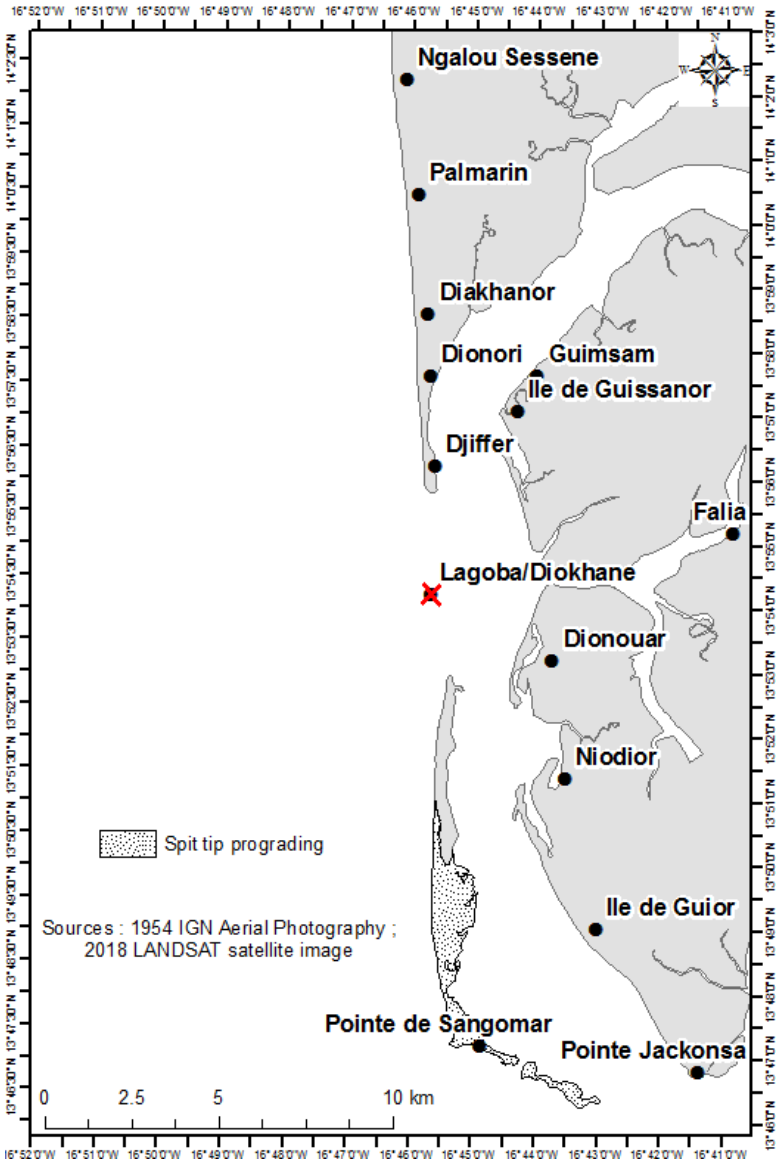
Ngalou Sessene
Palmarin
Diakhanor
Dionori
Guimsam
Ile de Guissanor
Djiffer
Falia
Lagoba/Diokhane
Dionouar
Niodior
Ile de Guior
Pointe de Sangomar
Pointe Jackonsa
Spit tip prograding
Sources : 1954 IGN Aerial Photography ;
2018 LANDSAT satellite image
0
2.5
5
10 km

Figure 6

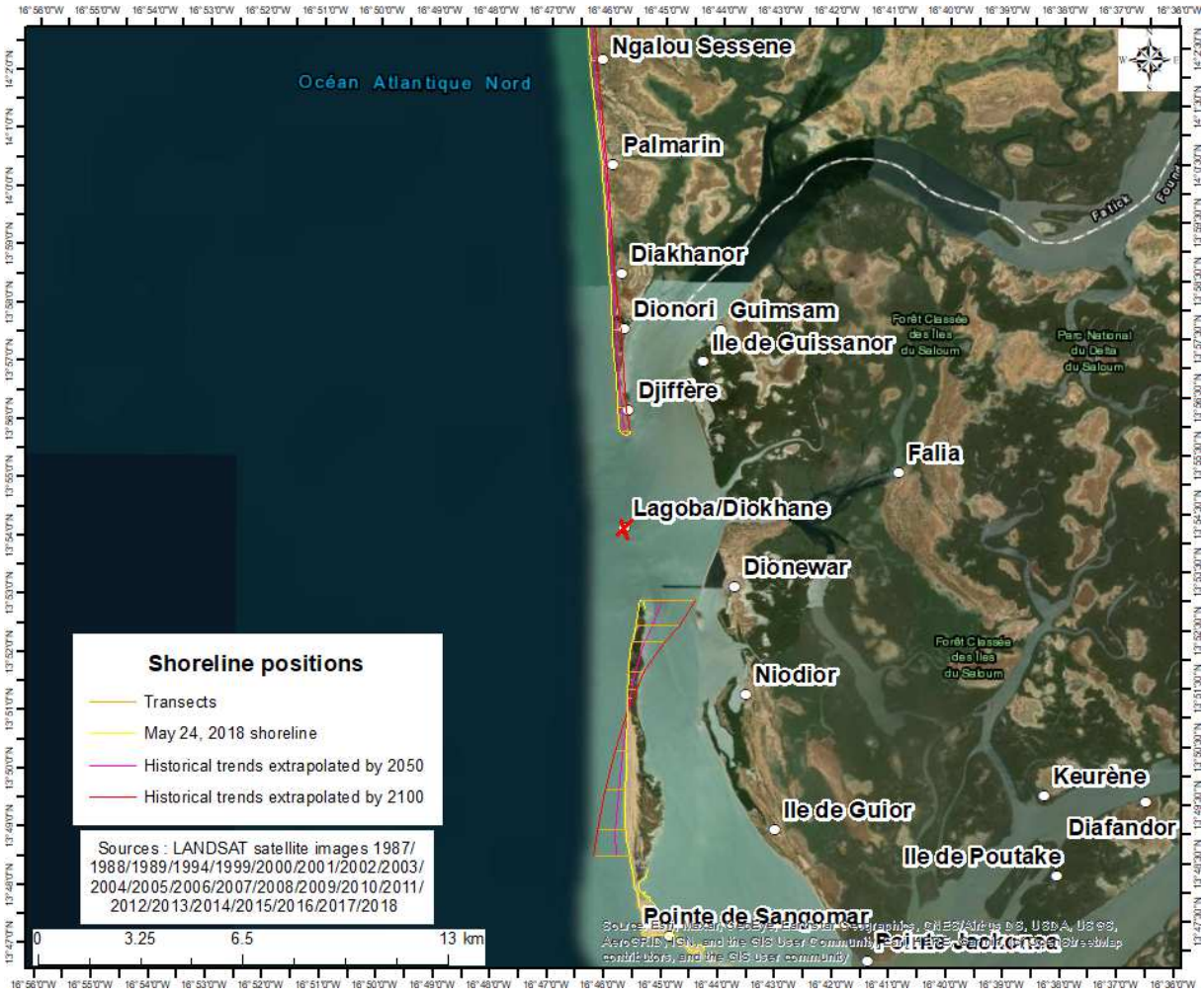
Océan Atlantique Nord
Ngalou Sessene
Palmarin
Diakhanor
Dionori
Guimsam
Ile de Guissanor
Djiffère
Falia
Lagoba/Diokhane
Dionewar
Niodior
Keurène
Ile de Guior
Diafandor
Ile de Poutake
Pointe de Sangomar
Shoreline positions
Transects
May 24, 2018 shoreline
Historical trends extrapolated by 2050
Historical trends extrapolated by 2100
Sources : LANDSAT satellite images 1987/ 1988/1989/1994/1999/2000/2001/2002/2003/ 2004/2005/2006/2007/2008/2009/2010/2011/ 2012/2013/2014/2015/2016/2017/2018
0
3.25
6.5
13 km

Figure 6

LIST OF TABLES

Table 1: Remote sensing data used

Data	Acquired date	Spatial resolution (meter)
IGN aerial photography	01/01/1954	01
CORONA satellite photograph	01/31/1968	02
LANDSAT satellite images	04/08/1984	30
	02/22/1985	30
	02/09/1986	30
	01/27/1987	30
	04/01/1987	30
	03/10/1988	30
	10/15/1989	30
	04/04/1994	30
	12/06/1999	15
	03/27/2000	15
	01/09/2001	15
	01/12/2002	15
	08/27/2003	15
	01/18/2004	15
	01/04/2005	15
	10/06/2006	15
	05/02/2007	15
	05/04/2008	15
	03/04/2009	15
	01/02/2010	15
	11/13/2011	15
	01/24/2012	15
	03/26/2013	15
	02/22/2014	15
	06/01/2015	15
	05/18/2016	15
	05/21/2017	15
	05/24/2018	15

Table 2: Shoreline evolution rate Uncertainty (in meters)

Period	Total error (m)	Annual error (m)
1954-1987	17	0.5
1987-2018	32.5	0.5